Computationally efficient simulation of extracellular recordings with multielectrode arrays

Thorbergsson, Palmi Thor; Garwicz, Martin; Schouenborg, Jens; Johansson, Anders J

Published in:
Journal of Neuroscience Methods

DOI:
10.1016/j.jneumeth.2012.08.011

2012

Computationally efficient simulation of extracellular recordings with multielectrode arrays

Palmi Thor Thorbergsson[1,2], Martin Garwicz[2,3], Jens Schouenborg[2,3], Anders J Johansson[1,2]

[1] *Department of Electrical and Information Technology, Lund University, Box 118, 22100 Lund, Sweden*

[2] *Neuronano Research Center, Lund University, Solvegatan 19, BMC F10, 22184 Lund, Sweden*

[3] *Department of Experimental Medical Science, Lund University, Solvegatan 19, BMC F10, 22184 Lund, Sweden*

E-mail: palmi.thor.thorbergsson@eit.lth.se

Abstract

In this paper we present a novel, computationally and memory efficient way of modeling the spatial dependency of measured spike waveforms in extracellular recordings of neuronal activity. We use compartment models to simulate action potentials in neurons and then apply linear source approximation to calculate the resulting extracellular spike waveform on a three dimensional grid of measurement points surrounding the neurons. We then apply traditional compression techniques and polynomial fitting to obtain a compact mathematical description of the spatial dependency of the spike waveform. We show how the compressed models can be used to efficiently calculate the spike waveform from a neuron in a large set of measurement points simultaneously and how the same procedure can be inversed to calculate the spike waveforms from a large set of neurons at a single electrode position. The compressed models have been implemented into an object oriented simulation tool that allows the simulation of multielectrode recordings that capture the variations in spike waveforms that are expected to arise between the different recording channels. The computational simplicity of our approach allows the simulation of a multi-channel recording of signals from large populations of neurons while simulating the activity of every neuron with a high level of detail. We have validated our compressed models against the original data obtained from the compartment models and we have shown, by example, how the simulation approach presented here can be used to quantify the performance in spike sorting as a function of electrode position.

Keywords: Extracellular recordings, Multielectrode arrays, Electrode movements Simulation, NEURON, Spike sorting, Spike detection

1. Introduction

Recently, there has been great interest in the development of brain machine interfaces (BMIs) with the aim to control prosthetic devices, conduct basic research on the central nervous system (CNS) and to treat the symptoms of neurological disease. One way of performing signal acquisition in BMIs is to use chronically implanted microelectrode arrays (Buzsáki, 2004) to measure the variation in extracellular potential resulting from discharges of action potentials in near by neurons. The extracellular representation of the action potential is usually referred to as a spike. Detecting spikes (Obeid and Wolf, 2004) in the extracellular signal and assigning them to their neurons of origin thus provides information about the activity patterns of individual neurons. The assignment part of that procedure is usually referred to as spike sorting (Lewicki, 1998). Since the performance in these processing steps is what determines the quality of the extracted information, the algorithms used for spike detection and spike sorting play a crucial role for the function of BMIs. Apart from the purely functional aspect, they are also important in the context of compressing the information contained in the neural signal for e.g. wireless transmission and/or memory-efficient storage for off-line analysis.

The development of algorithms for information extraction is an important aspect of BMI development. During design and evaluation of such algorithms, test signals are needed with a priori known information content, in which the spike times of each individual neuron in the recording are known and can be compared with the output of the algorithms. In addition to having a priori known characteristics, the test signals need to have realistic signal properties and these properties need to be controllable to some extent. Realism is important for the future applicability of the results and controllability is important since it allows the algorithm designer to perform studies of algorithm performance in a wide range of scenarios that might be encountered in future applications.

The approaches to obtaining adequate test signals can be roughly divided into three categories, (1) simultaneous intra- and extracellular recordings, (2) purely synthetic recordings and (3) hybrid recordings. In simultaneous intra- and extracellular recordings, the intracellular membrane potentials of the cells of interest are measured directly and since the signal-to-noise ratio in these is normally high, they can be used as ground truth when assessing the performance in spike detection and sorting applied to the extracellular signal (Harris, Henze, Csicsvari, Hirase and Buzsáki, 2000, Franke, Natora, Boucsein, Munk and Obermayer, 2010a). This class of test signals provides a high level of realism – the signals in question being

real. However, they lack in some practical aspects since keeping track of all true neuronal activity is difficult or even impossible in many cases. Besides these practical problems, controllability of the recording properties is limited. Despite these downsides, simultaneous intra- and extracellular recordings could serve as ultimate benchmark signals in later steps of the algorithm design process.

Purely synthetic recordings are based on mathematical models of the signal generation process. The mathematical models can in turn be divided into two subcategories, (1) models based on compartment models of the neurons and (2) models based on fixed spike templates. Compartment models rely on more or less detailed models of the mechanisms involved in producing the action potential across the cell membrane and of the resulting signal measured outside the cell (Smith and Mtetwa, 2007, Gold, Henze and Koch, 2007, Pettersen and Einevoll, 2008). The extracellular signal is calculated by considering the voltage contribution of each point on each contributing neuron at each given time instance. The amount of details captured by such models thus leads to high computational demand, which makes them unpractical when modeling large populations of neurons. However, they are realistic in the sense that they do capture the variations in the spike waveform's shape that arise when placing the recording electrode in different measurement points (Gold et al., 2007). This feature is of great importance when modeling recording setups with multiple and/or positionally unstable recording electrodes, both of which are important factors to consider during development of algorithms for spike detection and spike sorting in realistic scenarios.

Models based on fixed spike templates assume that the extracellular spike waveform measured from a given cell can be selected from a library of spike templates and then scaled according to the cells distance from the electrode (Thorbergsson, Jorntell, Bengtsson, Garwicz, Schouenborg and Johansson, 2009, Martinez, Pedreira, Ison and Quian Quiroga, 2009). Apart from the amplitude scaling, template based models do not capture any spatial variations in the shape of measured spike waveforms. Therefore, despite their computational simplicity, they are not suitable for simulating recordings with multiple and/or positionally electrodes. A possible solution to this limitation is to first employ a compartment model to calculate spike waveforms on a three dimensional grid of measurement points surrounding the neuron and then to interpolate the resulting waveforms to obtain waveforms in measurement points not lying on the simulation grid (Franke, Natora, Meier, Hagen, Pettersen, Linden, Einevoll and Obermayer, 2010b). Despite the increased level of realism introduced with this approach, it requires extensive waveform interpolation and may therefore not be suitable for simulating very large populations of neurons.

In hybrid recordings, synthetic spike trains are overlaid on real recordings of background noise (Pouzat, Mazor and Laurent, 2002). They are thus advantageous in the sense that they have highly realistic signal properties, but lack in controllability for the same reasons as simultaneous intra- and extracellular recordings.

Considering the above, there is an obvious trade-off between realism and computational complexity when selecting among the available modeling approaches. Despite the ever increasing availability of computational resources that indeed contributes to minimizing the impact of this trade-off, we reason that computational efficiency should be striven for. General availability to fast and simple ways of modeling complex recording scenarios would be of great value to researchers during the development of algorithms for signal processing. The possibility of quickly generating test data to match a specific recording setup would speed up the development phase and save valuable time.

In this paper, we present a novel, computationally and memory efficient approach to generating test signals that combines the detail of compartment models with the computational simplicity of template based models. To achieve this combination, we applied traditional dimensionality reduction techniques and polynomial fitting to compress the description of the spatial dependency in spike waveforms provided by compartment models. We used the *NEURON* simulation environment (Hines and Carnevale, 1997) to simulate an action potential in a compartment model of a CA1 pyramidal neuron originally modeled in (Gold, Henze, Koch and Buzsáki, 2006) and used in (Gold et al., 2007) and computed the extracellular spike waveforms on a three dimensional grid of measurement points using the line source approximation (LSA) (Holt and Koch, 1999). We then performed singular value decomposition (SVD) on the matrix containing the calculated spike waveforms and thereby obtained a set of basis waveforms describing the original spike matrix and their respective contributions to each of the original waveforms. Since most of the information describing the waveforms is contained in the first few (six) (Fee, Mitra and Kleinfeld, 1996a, Thorbergsson, Garwicz, Schouenborg and Johansson, 2010) components of this decomposition, we achieved dimensionality reduction (compression) by discarding all other components. The result of this was a trivariate field of six dimensional vectors, whose elements described the basis waveform weights as functions of the measurement point coordinates relative to the neuron in question. To obtain a compact description of the spatial dependency of the basis waveform weights, we individually fit the elements of the weight vector field to polynomial functions of the measurement point coordinates. The modeling procedure was carried out for four different neuronal compartment models (cases *A* to *D* in (Gold et al., 2007)) and the parameters of the compressed models were optimized for each neuron to provide a good match between the spike waveforms provided by the NEURON simulations and our compressed models. The models were implemented into an object oriented simulation tool, written in *Matlab*, that facilitates fast and realistic simulations of multielectrode recordings with arbitrary geometries. Model validation was performed by comparing spikes from the original NEURON simulations with spikes generated by our models in terms of shape and amplitude, as well as by examination of synthetic signals in terms of noise properties. The applicability of our approach was evaluated in an example application by estimating the performance in spike sorting as a function of electrode position.

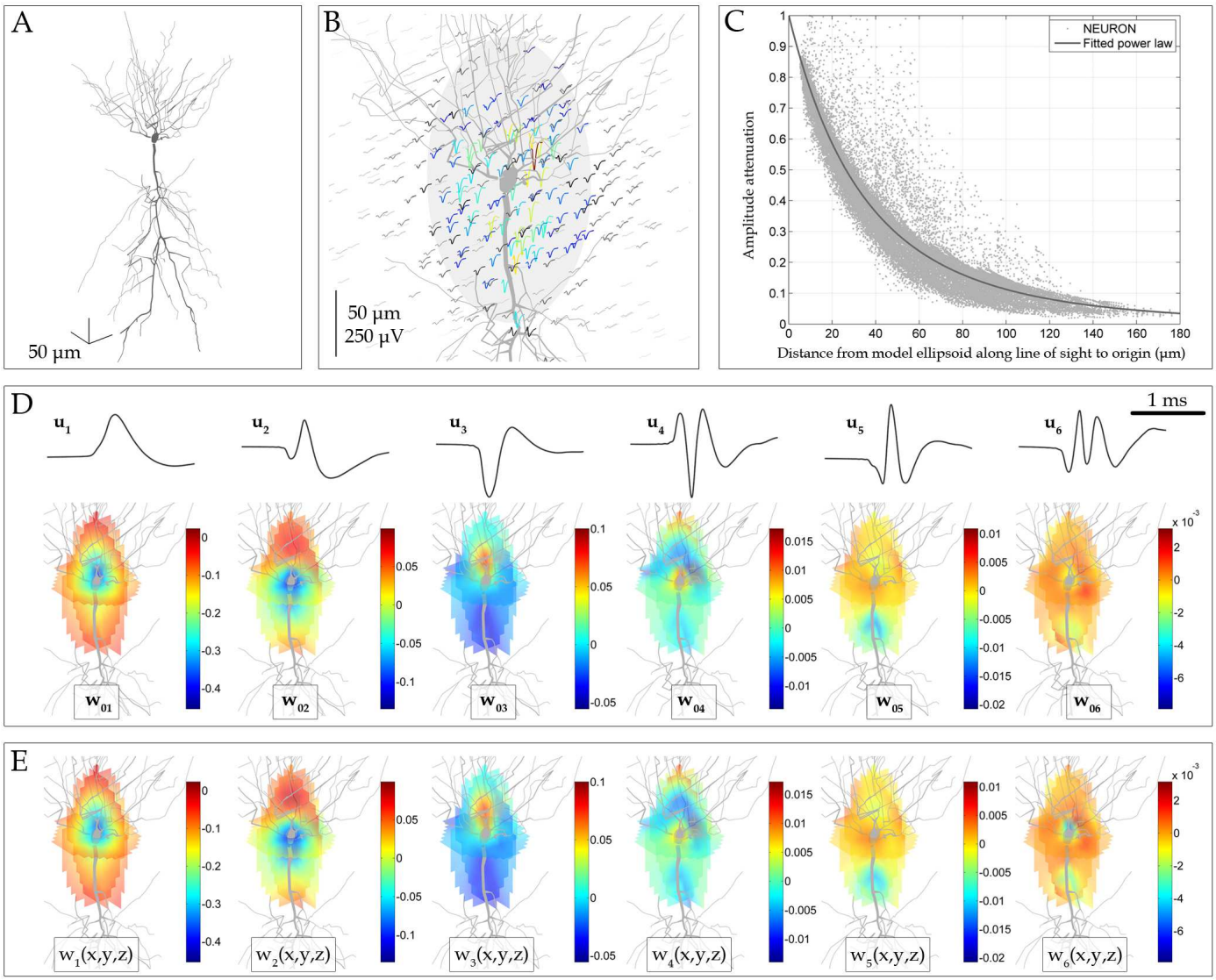

Figure 1: An illustration of the procedure of modeling the spatial dependency of the measured spike waveform for one of the neurons considered (neuron 1). (A) The CA1 pyramidal neuron model adopted from (Gold et al., 2007) was used to calculate extracellular spike waveforms in measurement points surrounding the neuron. (B) Spikes within an ellipsoid (overlaid ellipsoid) centered in the origin (cell soma) were used to derive the model. The ellipsoid was taken as the largest inscribed ellipsoid into the volume where spike amplitudes (maximum absolute amplitude) were at least A_{min} (typically around 20 μV. The spike waveforms are color coded according to their maximum amplitude (blue and red indicate low and high maximum amplitude respectively). (Note that for the sake of clarity, not all initial waveforms are shown here.) (C) Spikes with amplitudes below A_{min} (measured in points outside the model ellipsoid in (B)) were used to model the amplitude attenuation as a function of distance from the model ellipsoid along a line of sight from the measurement point to origin. (D) Singular value decomposition was used to find an orthonormal set of basis waveforms $\mathbf{u}_n$ and their weights $\mathbf{w}_{0n}$ describing spikes within the model ellipsoid. (E) The weight distributions were then individually fit to trivariate polynomial functions of measurement point coordinates, $w_n(x, y, z)$.

2. Methods

2.1. Neuron models

Figure 1 illustrates the procedure we followed to derive the compressed neuron models. We used the CA1 pyramidal neuron compartment models employed in (Gold et al., 2007) as a starting point for obtaining spike waveforms on a three dimensional grid of measurement points around the neuron. An action potential was simulated in the model neuron with four different ionic channel densities (referred to as cases *A* to *D* in (Gold et al., 2007), referred to here as *neuron 1* to *neuron 4*) and the extracellular spike waveform was calculated in measurement points on a three dimensional grid surrounding the neuron using the line source approximation (LSA) (Holt and Koch, 1999). The measurement points were distributed within a volume of $140 \times 140 \times 140$ μm and the spacing between the points was varied between 5 and 20 μm in each dimension (x, y, z). Close to the cell soma ($\{x, y, z\} \leq \{60\}\mu m$), the spacing was 5 μm and further away, it was successively increased to 10 μm and 20 μm. This resulted in a total of 42.875 initial measurement points.

To verify that this measurement point density was sufficient, we calculated the correlation coefficients between spike waveforms in all pairs of measurement points within a distance of 60 μm from the origin and then calculated the mean and standard

deviation of the correlation coefficient as a function of distance between measurement points. The mean minus one standard deviation was above 0.99 for all neurons at a measurement point distance of 5 μm. At a measurement point distance of 20 μm, the mean minus one standard deviation of correlation coefficients was above 0.97. This indicates that the chosen measurement point densities were adequate to capture the spatial variation in spike waveforms.

The first step in the modeling procedure for each of the neurons was to find a volume within which the model would be derived. For points outside that volume, amplitude scaling was applied (discussed later in this section). The volume was taken as an ellipsoid, concentric with the cell soma, inscribed into the volume bounded by the measurement points in which the spike amplitude exceeded a case-specific value of A_{min}. Spike amplitude was defined as the maximum absolute amplitude of the spike waveform. Finding the optimal value of A_{min} was part of a model selection procedure that is discussed later in this section. Having identified the model ellipsoid, spikes within the ellipsoid were arranged into columns of the spike matrix $\mathbf{S}_0$. $\mathbf{S}_0$ was then decomposed using singular value decomposition (SVD) according to

$$\mathbf{S}_0 = \mathbf{U}\mathbf{\Sigma}\mathbf{V}^T = \mathbf{U}\mathbf{W}_0 \tag{1}$$

where the columns of the matrix $\mathbf{U}$ contain an ordered set of orthonormal basis waveforms describing the original spike matrix $\mathbf{S}_0$ and the columns of the matrix product $\mathbf{\Sigma}\mathbf{V}^T = \mathbf{W}_0$ contain the contributions (weights) of each of the basis waveforms in constructing the original set of spike waveforms in $\mathbf{S}_0$. Since most of the spike waveform variation is described by the first few basis waveforms, we discarded all but the first six components of the decomposition to achieve a dimensionality reduction (Fee et al., 1996a, Thorbergsson et al., 2010). In order to assure that no information about spike waveform variability was lost by discarding the other components, we calculated the amount of total variance described by the first six components as

$$p_6 = \frac{\sum_{n=1}^{6} \sigma_n^2}{\sum_{n=1}^{N} \sigma_n^2} \tag{2}$$

where σ_n is the n-th singular value. This ratio was larger than 0.99 in all cases, indicating that the first six components adequately described the waveform variability.

We now modeled the weight of the n-th basis waveform as a trivariate polynomial function of the measurement point coordinates (x, y, z) in a coordinate system with origin in center of the cell soma, i.e.

$$w_n(x, y, z) = \sum_i c_{i_n} x^{\mathbf{e}_{i,1}} y^{\mathbf{e}_{i,2}} z^{\mathbf{e}_{i,3}} \tag{3}$$

where c_{i_n} is the i-th polynomial coefficient and $\mathbf{e}$ is a matrix whose i-th row contains the i-th combination of x, y and z exponents included in the model. For instance, if the i-th polynomial term is $c_i x^3 y^2$, the corresponding row in the exponent matrix $\mathbf{e}$ is [3 2 0]. The exponent matrix was constructed by assuming maximum orders of pure terms (including only one of the three coordinates) and mixed terms (including more than one of the three coordinates). These orders were referred to as N_{pure} and N_{mixed} and together with the minimum spike amplitude A_{min}, they determined the model properties and were selected to provide a good match between original and modeled spike waveforms (discussed later in the current section).

The polynomial fitting was performed by solving the equation system

$$(\mathbf{AD})\mathbf{C} = \mathbf{W}_0$$

$$\begin{bmatrix} x_1^{\mathbf{e}_{1,1}} y_1^{\mathbf{e}_{1,2}} z_1^{\mathbf{e}_{1,3}} & x_1^{\mathbf{e}_{2,1}} y_1^{\mathbf{e}_{2,2}} z_1^{\mathbf{e}_{2,3}} & \cdots & x_1^{\mathbf{e}_{I,1}} y_1^{\mathbf{e}_{I,2}} z_1^{\mathbf{e}_{I,3}} \\ x_2^{\mathbf{e}_{1,1}} y_2^{\mathbf{e}_{1,2}} z_2^{\mathbf{e}_{1,3}} & x_2^{\mathbf{e}_{2,1}} y_2^{\mathbf{e}_{2,2}} z_2^{\mathbf{e}_{2,3}} & \cdots & x_2^{\mathbf{e}_{I,1}} y_2^{\mathbf{e}_{I,2}} z_2^{\mathbf{e}_{I,3}} \\ \vdots & \vdots & \cdots & \vdots \\ x_L^{\mathbf{e}_{1,1}} y_L^{\mathbf{e}_{1,2}} z_L^{\mathbf{e}_{1,3}} & x_L^{\mathbf{e}_{2,1}} y_L^{\mathbf{e}_{2,2}} z_L^{\mathbf{e}_{2,3}} & \cdots & x_L^{\mathbf{e}_{I,1}} y_L^{\mathbf{e}_{I,2}} z_L^{\mathbf{e}_{I,3}} \end{bmatrix} \mathbf{D} \cdots$$

$$\begin{bmatrix} c_{1_1} & c_{1_2} & \cdots & c_{1_6} \\ c_{2_1} & c_{2_2} & \cdots & c_{2_6} \\ \vdots & \vdots & \cdots & \vdots \\ c_{I_1} & c_{I_2} & \cdots & c_{I_6} \end{bmatrix} = \begin{bmatrix} w_{1_1} & w_{1_2} & \cdots & w_{1_6} \\ w_{2_1} & w_{2_2} & \cdots & w_{2_6} \\ \vdots & \vdots & \cdots & \vdots \\ w_{L_1} & w_{L_2} & \cdots & w_{L_6} \end{bmatrix} \tag{4}$$

where L is the number of measurement points used in the fitting, I is the total number of polynomial terms in the fitted model, $\mathbf{A}$ is the multivariate Vandermonde matrix, $\mathbf{D}$ is an $I \times I$ diagonal matrix whose i-th diagonal element is the reciprocal of the Euclidean norm of the i-th column of $\mathbf{A}$, $\mathbf{C}$ is the coefficient matrix to be estimated (c_{i_p} is the estimated polynomial coefficient of the i-th term for the p-th basis waveform) and $\mathbf{W}_0$ is the original weight matrix (w_{l_p} is the weight of the p-th basis waveform in the l-th measurement point). The purpose of the matrix $\mathbf{D}$ was to scale the columns of the Vandermonde matrix to improve the conditioning of the problem. The number of measurement points was in all cases larger than the number of polynomial terms (i.e. $L > I$). The equation system was thus overdetermined and solving it yielded a least-squares solution.

For measurement points outside the model ellipsoid (in the far-field of the neuron) we assumed the measured spike waveform to be an attenuated version of the spike waveform measured in the point of intersection between the model ellipsoid and the line of sight from the measurement point to the origin. We assumed the attenuation g to be a power-law function of the distance r between the measurement point and the point of intersection, i.e.

$$g(r) = \frac{1}{(1 + a_{far} r)^{b_{far}}}. \tag{5}$$

The coefficients a_{far} and b_{far} were estimated by fitting the amplitudes of spikes with amplitudes below A_{min} to a power-law function of their corresponding measurement point distances (along the line of sight to origin) to the model ellipsoid. The power-law was estimated assuming the distance r to be in micrometers. Thus, the unit of the coefficient a_{far} is $[\mu m^{-1}]$. The form of the power-law was chosen to provide an attenuation of 1 at a distance of 0 from the model ellipsoid. This way of modeling the spike waveforms in the far-field assured a continuous variation in the spike waveform when moving the electrode out of the model ellipsoid and between points outside the model ellipsoid.

As mentioned before, each neuron model was characterized by three parameters – A_{min}, N_{pure} and N_{mixed}. For each of the neurons, we performed the modeling procedure for all combinations of model parameters in the ranges $A_{min} \in [16, 26]\mu V$ (steps of 2 μV), $N_{pure} \in [10, 24]$ (steps of 1) and $N_{mixed} \in [2, 8]$ (steps of 2), resulting in a total of 360 models per neuron. The spike waveforms calculated by each of the models were compared with those obtained from the original NEURON simulations and a score was assigned to each model based on how the waveforms matched in terms of shape and amplitudes. To lower the computational demand during the comparison, we selected two random sets of measurement points to use in the comparison – 20% of the entire set of points within the near field (NF, inside the model ellipsoid) and 20 % of the entire set of points in the far field (FF). The following metrics were calculated to obtain the model scores:

- e_{NF_1} = 1 − mean(correl. coeffs. between spikes in NF)
- e_{NF_2} = std(correl. coeffs. between spikes in NF)
- e_{NF_3} = mean(abs. diff. between spike amplitudes in NF)
- e_{NF_4} = std(abs. diff. between spike amplitudes in NF)
- e_{FF_1} = mean(abs. diff. between spike amplitudes in FF)
- e_{FF_2} = std(abs. diff. between spike amplitudes in FF)

The metrics were normalized to range from 0 to 1, 0 indicating the closest match and 1 the worst match. Based on the normalized metrics, the following model scorese were then defined ($\hat{}$ denotes the normalized metrics):

- Near field score:

$$s_{NF} = \sqrt{\hat{e}_{NF_1}^2 + \hat{e}_{NF_2}^2 + \hat{e}_{NF_3}^2 + \hat{e}_{NF_4}^2} \quad (6)$$

- Far field score:

$$s_{FF} = \sqrt{\hat{e}_{FF_1}^2 + \hat{e}_{FF_2}^2} \quad (7)$$

- Total score:

$$s_{tot} = \sqrt{s_{NF}^2 + s_{FF}^2} \quad (8)$$

We wanted to select a model that, apart from minimizing the total score s_{tot}, also minimized the difference between the near and far field scores. Thus, we selected the model that minimized the function

$$E = \sqrt{\Delta_s^2 + \hat{s}_{tot}^2} \quad (9)$$

where Δ_s is the normalized (0 to 1) absolute difference between near- and far-field scores and $\hat{s}_{tot}$ is the normalized (0 to 1) total score. This procedure consistently resulted in the automatic selection of a model that provided a high overall match with the original data while simultaneously performing well in both the near- and far-field.

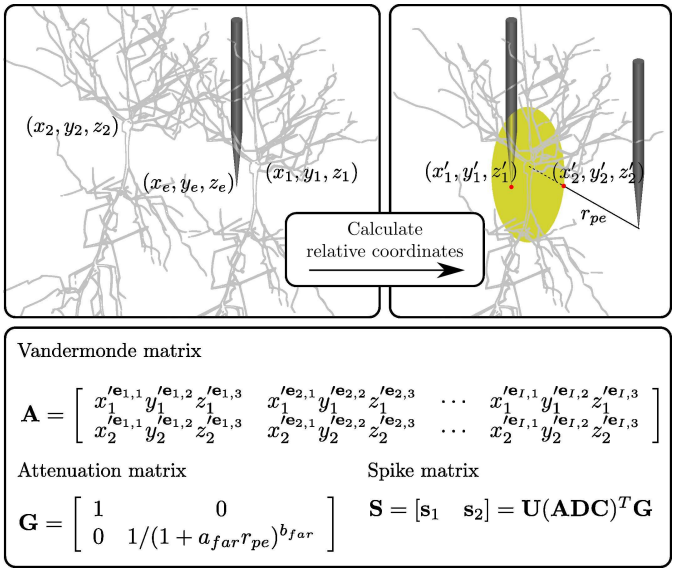

Figure 2: An illustration of how the derived models can be used to calculate the extracellular spike waveforms from two neurons measured with a single electrode. In the original coordinate system, the electrode is located in (x_e, y_e, z_e) and the neurons are located in (x_1, y_1, z_1) and (x_2, y_2, z_2) respectively. Assuming that the neurons are of the same type (share the same neuron model), the first step is to calculate the positions of the electrode relative to the two neurons, (x'_n, y'_n, z'_n). Relative measurement points inside the model domain of the neuron (yellow ellipsoid) are left unchanged (x'_1, y'_1, z'_1) and measurement points outside the model domain are replaced with the point of intersection between the model ellipsoid and a line of sight to origin. In the first case, the attenuation is set to 1 (element (1,1) in the attenuation matrix **G**) and in the second case it is set to $1/(1 + a_{far} r_{pe})^{b_{far}}$ where a_{far} and b_{far} are estimated model coefficients and r_{pe} is the distance of the relative measurement point from the model ellipsoid along the line of sight to origin before it was replaced with the intersection point. The Vandermonde matrix is constructed using the exponent matrix **e** (obtained from the neuron model) and relative measurement points and finally the matrix **S** containing the spike waveforms in its columns is calculated with a simple matrix multiplication. The basis waveform matrix **U** and model coefficient matrix **DC** are parts of the derived model.

Having selected the best model for a specific neuron, the model description was saved for implementation into the simulation algorithm. The main parameters included in the model were the basis waveforms (sampled at 25 kHz), the matrix product **DC**, the exponent matrix **e**, the axial radii of the model ellipsoid and the coefficients of the far-field attenuation power-law. The model parameters A_{min}, N_{pure}, N_{mixed} were also included for descriptive purposes. The model files were typically around 40kB of size which is three orders of magnitude smaller than the original spike matrix obtained from the NEURON simulations that were typically around 31MB.

The stored model parameters could now be used to efficiently calculate spike waveforms from neurons in a large set of arbitrary measurement points. Using the same procedure, we could also calculate the spike waveforms from a large set of neurons sharing the same neuron model in a single measurement point. Figure 2 illustrates this procedure. Assuming that we have a single electrode placed in (x_e, y_e, z_e) and N neurons where the n-th neuron is placed in (x_n, y_n, z_n), the waveforms from the neurons can be calculated in the following way:

Step 1: Calculate the relative positions of the electrode

For every neuron placed in (x_n, y_n, z_n), calculate the position of the electrode relative to that neuron, i.e.

$$(x'_n, y'_n, z'_n) = (x_e, y_e, z_e) - (x_n, y_n, z_n). \quad (10)$$

The problem is now that of calculating the spike waveform from a single neuron in N separate measurement points where the n-th point is (x'_n, y'_n, z'_n).

Step 2: Construct Vandermonde and attenuation matrices

For every (relative) measurement point, (x'_n, y'_n, z'_n), check if the point is inside or outside the model ellipsoid by evaluating the quantity

$$r_{check} = \frac{x'^2_n}{r^2_{e_x}} + \frac{y'^2_n}{r^2_{e_y}} + \frac{z'^2_n}{r^2_{e_z}} \quad (11)$$

where $r_{e_\cdot}$ is the radius of the model ellipsoid along the $\cdot$-axis. If r_{check} is larger than 1, the point is outside the model ellipsoid and is thus replaced with the point of intersection between the line of sight to origin and the model ellipsoid. If r_{check} is smaller than or equal to 1, the point is inside the model ellipsoid and is left unchanged. If the point is outside the model ellipsoid, the $n-th$ diagonal element of the $N \times N$ diagonal attenuation matrix $\mathbf{G}$ is set to $1/(1 + a_{far} r_{pe})^{b_{far}}$ where r_{pe} is the distance of the point to the ellipsoid along the line of sight to origin. If the point is inside the model ellipsoid, the attenuation value is set to 1. After performing the above check and replacing/keeping the relative measurement point coordinates, the l-th element of the n-th row of the Vandermonde matrix $\mathbf{A}$ is set to $x_n'^{\mathbf{e}_{l,1}} y_n'^{\mathbf{e}_{l,2}} z_n'^{\mathbf{e}_{l,3}}$.

Step 3: Calculate the spike matrix

The spike matrix $\mathbf{S}$ whose n-th column contains the modeled spike waveform from the n-th neuron can now be calculated as

$$\mathbf{S} = \mathbf{U}(\mathbf{ADC})^T \mathbf{G}. \quad (12)$$

Note that the above procedure assumes that all neurons share the same neuron model. If the volume to be simulated contains several types of neurons, the entire population of neurons can be divided into subpopulations according to type and the subpopulations can then be treated individually according to the above procedure.

2.2. Firing Models

Three models were implemented for generating spike times – gamma distributed inter spike intervals, bursting and correlated spike trains. In the current implementation, each neuronal population is assumed to have the same basic firing model, although the model parameters are set individually for each neuron. For instance, a population of neurons can have gamma distributed inter spike intervals, but each neuron in the population has an individual mean firing rate. For bursting neurons, inter-burst-intervals were assumed to be gamma distributed and the number of spikes within a burst was assumed to follow a Poisson distribution (Heeger, 2000). Changes in the spike waveform during a bursting period were not accounted for. We included the methods in (Macke, Berens, Ecker, Tolias and Bethge, 2009) to generate correlated spike trains. Having used firing models to generate spike times for every neuron in the simulation volume, the measured signal at each recording channel was assembled by adding the calculated spike waveforms from each neuron at that channel at the spike times of that neuron in the same manner as described in (Thorbergsson et al., 2009).

2.3. Noise Models

We assumed noise to consist of two components, namely the spiking activity of distant neurons and thermal noise caused by random charge movements. This is a common way of modeling noise in extracellular recordings (Martinez et al., 2009, Thorbergsson et al., 2009, Lempka, Johnson, Moffitt, Otto, Kipke and McIntyre, 2011). The thermal noise amplitude depends on recording bandwidth, temperature and input resistance of the recording electrode (Pettai, 1984, Lempka et al., 2011) and we assumed it to be zero-mean normally distributed with a standard deviation determined by these parameters. We used the results presented in (Lempka et al., 2011) to derive a quantitative model for setting the standard deviation. We approximated an extrapolation of the resistive part of the electrode impedance for an electrode size of 177 μm^2 to include frequencies from 100 Hz to 50 kHz and obtained an estimation of the power spectral density,

$$P(f) = 2kTR(f) \quad (13)$$

where k is the Boltzmann constant, T is temperature in Kelvin (set to 37°C) and $R(f)$ is the resistance as a function of frequency, f. The standard deviation of the thermal noise, $\sigma_{N_{th}}$, was then obtained as a function of recording bandwidth by taking the square root of the integral of the power spectral density over the recording bandwidth,

$$\sigma_{N_{th}}(f_B) = \sqrt{\int_0^{f_B} P(f) df} \quad (14)$$

where f_b is the recording bandwidth. A general description of this relationship was obtained by fitting $\sigma_{N_{th}}$ to a power-law function of $\log(f)$,

$$\sigma_{N_{th}}(f_B) = a_t \log(f_B)^{b_t}. \quad (15)$$

Physiological background noise was assumed to come from the spiking activity of distant neurons. To be able to make a distinction between the noise component of the signal and the spiking activity, we assumed the noise contributing neurons to be located at a minimum distance of r_i from the electrode (or origin) and we assumed them to have random mean firing rates selected from a uniform distribution between 1 and f_u spikes/second. The minimum distance r_i and the upper level of firing rates were then used to set the background noise level (see Section 2.5). Due to the computational efficiency of the methods described in Section 2.1, we were able to generate the background noise using the relative positions of the noise

contributing neurons, thus employing the entire variability in spike waveforms described by the neuron models in the noise generation process also. Thus, although we make a distinction between noise- and signal contributing neurons from the perspective of the recorded signal, the two categories of neurons were treated in exactly the same way in the simulation process. We did, however, include the possibility of not storing the true spike times for neurons far away from all recording electrodes, thus further decreasing the memory requirements and simulation time (See section 2.4).

2.4. Simulator Implementation

The simulator was implemented in *Matlab* using object oriented programming. We assumed the core components of the simulation to be the neuronal populations contributing to the signal, the array of electrodes recording the signals and a recorder that kept track of ground truth data and recorded signals. This abstract structure was implemented with three object models, one for each of these core components. A brief description of the properties of each object model follows:

The neuron class
An object of the neuron class contains information about the properties of a population of neurons that share the same model, both in terms of the spatial dependency of spike waveforms and firing times. The information contained is the absolute coordinates of the neurons, the volume density within the population, a description of the volume containing the population, the spike model associated with the population and the firing statistics and spike times for the individual neurons. The neuron class has methods to generate spike times for its neurons based on the duration of the recording and the individual neuronal firing statistics. In order to simulate a specific recording setup where several types of neurons (in terms of spike and/or firing models) exist in specific regions, one neuron object is constructed for each population within the volume.

The electrode class
An object of the electrode class contains the absolute coordinates of each electrode site and the spike waveforms from every neuron in every population calculated at the position each electrode. The electrode class contains methods to calculate the spike waveforms and to assemble the signal measured at each electrode site from the calculated spike waveforms and the spike times contained by the neuron objects.

The recorder class
An object of the recorder class contains information about the structure of the HDF5 simulation file (see following paragraph) where the simulation data is stored and methods to interact with the simulation file during and after simulation. This interaction includes writing the information contained in and generated by the neuron and electrode objects to the simulation file as well fetching the information once it is written to the file. The recorder class also contains several methods to visualize the simulation results.

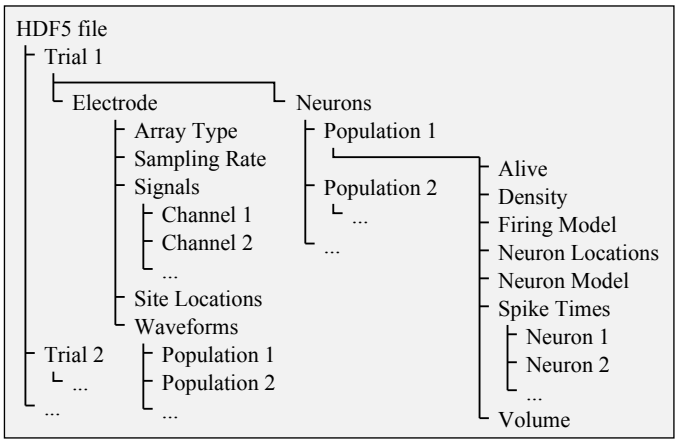

Figure 3: An illustration of how simulation data is organized into HDF5 files. In order to lower memory requirements, all information is written to the HDF5 file as soon as it becomes available during simulation. Upon starting a simulation, a new HDF5 file is created and a recorder object that provides read/write access to it is constructed. After the simulation is complete, it can be loaded in read-mode by calling the recorder object constructor function with the file name as input. The functions implemented in the recorder object provide fast access to all simulation data in a database-query type of way.

In order to minimize memory requirements, we employed the HDF5 (*Hierarchical Data Format* file format (The HDF Group, 2012) for data storage during simulation. The HDF5 file format is suitable for fast read and write access for large and complex datasets and allows database-like queries to be made once the file structure has been defined. Figure 3 illustrates the HDF5 file structure that we designed. When a *recorder object* is constructed in write mode, it creates a new HDF5 file for the recording that is to be simulated and then it provides read/write access to the simulation data as long as it exists. After simulation, a recorder object can be constructed in read mode with the name of the simulation file as input, thus allowing quick post-simulation access to all simulation data. The recorder object also allows for instance quick plotting of the synthetic signals, true spike waveforms as measured at the individual recording channels and the 3D geometry of the simulated volume.

2.5. Validation

The validity of our results was examined in terms of similarity between original and model-generated spike waveforms and noise properties of simulated recordings. The shapes of the spike waveforms were visually compared within the near-field (inside the model ellipsoid). Spike amplitude (maximum absolute amplitude) was examined as a function of distance from origin (cell soma) and by qualitative comparison of spike amplitude fields around the neuron. The amplitude fields were visualized by plotting three-dimensional isosurfaces around the neurons at spike amplitudes of 25, 50 and 100 μV. The spike amplitude distributions for the original data (NEURON generated spikes) were estimated by selecting approximately half of the original measurement points at random and calculating the

mean and standard deviation of spike amplitudes in measurement points within 10 μm wide distance bins from the origin. For the spikes generated with our models, we used the same coordinates as for the true spikes, but with a small random shift. The random shift was introduced in order to make sure that the model captured the overall appearance of the amplitude distribution, even in measurement points that were off the original measurement point grid. In addition, evaluating the amplitude distribution in off-grid measurement points would reveal any potential problems with "over-fitting". The spike amplitude isosurfaces were estimated in the same way, i.e. using an equally large random set of measurement points and applying a random shift for the model-generated spikes. Apart from these comparisons, we also included the metrics calculated during the model selection procedure (Section 2.1) as validity measures.

Noise properties of simulated single channel recordings were examined in terms of sample histograms, normalized power spectral density and standard deviation of noise. We assumed the noise properties to be mainly determined by the radius of the "silent volume" around the recording electrode and the distribution of firing rates among the neurons contributing to the background noise (see Section 2.3). To estimate the noise properties as functions of these parameters, we set up a recording scenario with a single electrode placed in the origin and we then created four populations of noise neurons (one population of each type of neuron) surrounding the electrode. The noise neurons were placed at random positions within a hollow cylindrical volume centered along the z-axis. The outer boundaries of the volume were defined by a cylinder with a radius of 250 μm and z between -250 μm and 250 μm. The inner boundaries were defined by a cylinder with a variable radius r_i ranging from 50 μm to 150 μm and z between -150 μm and 250 μm. Assuming a neuronal density of 9.5×10^6 neurons/cm^3 (Lempka et al., 2011), gamma distributed inter-spike intervals (Thorbergsson et al., 2009) and a minimum firing rate of 1 spike/second, we synthesized 30 second long noise recordings while varying the minimum distance of noise contribution neurons, r_i, and the upper limit of firing rates, f_u. r_i and f_u were varied between 50 and 150 μm and 5 and 80 spikes/second respectively. The recordings were synthesized at a sampling rate of 100 kHz, but were downsampled to 25 kHz and then bandpass filtered (300 Hz to 5 kHz). We then estimated the power spectral density using Welch's method, the sample amplitude histogram and the standard deviation of the resulting noise signal. Thermal noise was included since that was assumed to be an inevitable part of the recorded noise in a real situation. Besides allowing us to compare the noise properties of our simulator with those of previously reported simulators, this analysis provided basic means for controlling the noise properties by altering the parameters mentioned above.

2.6. Application Example: Spike Sorting Performance

The applicability of our work was evaluated by an example application in which we explored the effects of electrode position on the performance in spike sorting. Noise neurons were created in the same manner as described in the previous section. The inner radius of the the hollow noise cylinder was set to $r_i = 150 \mu m$ and the upper limit of noise neuron firing rates was set to 50 Hz. Four target neurons (one of each type, cell 1 to 4) were placed in $(10, 20, -2)$ μm, $(-2, 18, 20)$ μm, $(-20, -5, 10)$ μm and $(16, -13, 15)$ μm respectively (Cartesian coordinates of cells 1 through 4, μm). All target neurons had gamma distributed inter-spike intervals and random mean firing rates between 1 and 10 Hz. Nineteen electrodes were placed along the z axis ($x = y = 0$) at positions ranging from $z = -30 \mu m$ to $z = 60 \mu m$ (5 μm spacing) and a 60 second long recording was synthesized (a close-up of the electrodes and the target neurons is shown in Figure 7 A).

Having obtained the HDF5 simulation file, we used the interface provided by the *recorder* class to extract the spike waveforms for each of the target neurons at each of the electrode sites at the known spike times. We thus obtained nineteen sets of extracted spike waveforms, each corresponding to one electrode position. The spikes from each position were then sorted separately and the sorting accuracy was estimated. Principal component analysis (PCA) (Lewicki, 1998) was used to extract spike features and the first two principal component weights (PC 1 and PC 2) were used to perform sorting of the spikes using K-means clustering (Duda, Hart and Stork, 2001). Since we were only interested in comparing the performance in spike sorting while varying the electrode position, and not the absolute performance of the selected spike sorting algorithm, we provided the true number of clusters (4 cells) to the K-means algorithm as input. We only employed the first two principal component weights in the clustering since that allowed for a straight forward visual interpretation of the spike sorting performance in terms of a two dimensional illustration of the PCA feature space representation of the spikes (Figure 7 D).

Having obtained the sorting results for a given set of spikes (a given position), the spike sorting accuracy was estimated in terms of true and false positive classification rates per cell (P_{TP} and P_{FP} respectively) and an overall sorting accuracy (P_{ID}). The true positive classification rate (P_{TP}) for a given cell in a given electrode position was calculated as the ratio between the number of spikes correctly assigned to that cell and the total number of spikes truly coming from that cell. False positive classification rate (P_{FP}) for a given cell in a given electrode position was calculated as the ratio between the number of spikes wrongfully assigned to that cell and the total number of spikes truly coming from any other cell. Overall spike sorting accuracy (P_{ID}) for a given electrode position was calculated as the ratio between the overall number of correctly classified spikes and the total number of spikes.

3. Results and Discussion

3.1. Model Parameters

The estimated neuron model parameters are summarized in Table 1. The minimum spike amplitude (A_{min}) included ranged from 18 to 24 μV, and the maximum degree of pure and mixed polynomial terms was 10 to 24 and 6 to 8 respectively. The model domain ellipsoid had a radius of approximately 45 to 65 μm in the $x - y$ plane and 104 to 142 along the z axis. A maximum distance of 50 μm between a neuron and the electrode is

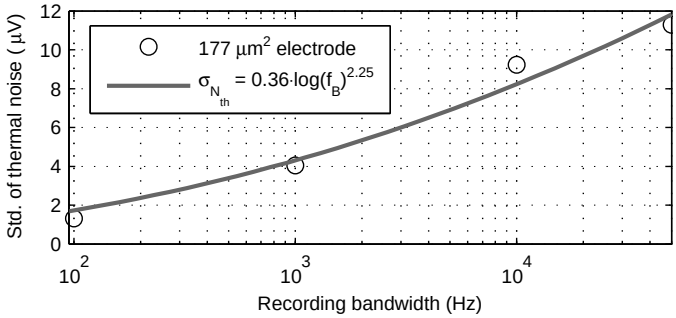

Figure 4: The standard deviation of thermal noise, $\sigma_{N_{th}}$ at a temperature of 37°C fitted to a power law function ($R^2 = 0.98$) of the logarithm of recording bandwidth f_B for an electrode of 177 μm^2 extrapolated from (Lempka et al., 2011).

assumed for the neuron's spikes to be distinguishable from the background noise (Buzsáki, 2004). The model ellipsoids of all neurons approximately cover that range. For neuron 4, the *x*-axial radius is below 50 μm, which is explained by the smaller (in the $x - y$ directions) spike amplitude field for neuron 4 (see Figure 5 B), which in effect would lower the 50 μm distance threshold mentioned before.

The estimated power law describing the standard deviation of thermal noise as a function of recording bandwidth is shown in Figure 4. The parameters of the fitted power law according to Equation 15 where $a_t = 0.36$ and $b_t = 2.25$. The coefficient of determination between the standard deviations adopted from (Lempka et al., 2011) and the fitted power-law was $R^2 = 0.98$, indicating a good match.

3.2. Validation

3.2.1. Spike Waveforms and Amplitude

All four models provided a good match in terms of spike waveforms and spike amplitudes when compared to the original data. Figure 5 A shows the true spike waveforms (black) and spike waveforms calculated by the neuron models (red dots) in an example set of measurement points. By visual inspection of these waveforms, we see that the models produce essentially identical waveforms to those generated by the original NEURON simulations. Mean correlation between true and modeled spike waveforms in the near field was larger than 0.99 (standard deviation < 0.02) for all neurons (metrics e_{NF_1} and e_{NF_2}). Mean amplitude deviation in the near field was below 2 μV (standard deviation < 5μV) for all neurons (metrics e_{NF_3} and e_{NF_4}). Mean amplitude deviation in the far field was below 0.4 μV (standard deviation < 2.1μV) for all neurons (metrics e_{FF_1} and e_{FF_2}).

Figure 5 B shows the spike amplitude isosurfaces (25, 50 and 100 μV) for NEURON generated spikes and spikes generated by the compressed models. In all four cases, the compressed models capture the major features of the amplitude fields at all three amplitudes examined. This also applies to most "non-regular" features, such as the surface irregularities at the top of the 25 μV surface for neuron 4 and the following of the 50 μV surface along the axon for neuron 4.

Figure 5 C shows the mean and standard deviation of spike amplitudes as a function of distance from the origin (cell soma) within 10 μm wide distance bins. Also here, there is no noticeable difference between the original spike amplitudes and those produced by our models. In all cases, the models capture most of the local variations in spike amplitudes (for instance at local decrease in standard deviation of spike amplitudes at 90 to 100 μm for neuron 3). These local variations are caused by the non-uniform structure of the neuron, i.e. some points far away from the soma are in fact very close to other parts of the neuron.

3.2.2. Noise Properties

Figure 6 shows the noise level (σ_N), power spectral density (PSD) and sample histogram as functions of the upper limit of noise neuron firing rates, f_u, and minimum distance of noise contributing neurons, r_i. The figure shows that by varying those parameters we can control the amplitude and spectral properties of the recording noise. The figure also shows that we can obtain a good match with previously reported spectral properties and sample histograms (Fee, Mitra and Kleinfeld, 1996b, Martinez et al., 2009).

Increasing the maximum firing rate of noise neurons and decreasing the minimum distance to them increased the noise level and concentrated the noise towards the lower part of the spectrum, in which most of the spike energy is contained.

At large distances to the noise neurons (rightmost column in Figure 6), the change in noise neuron firing rate had less impact on the noise amplitude than at small distances (leftmost column in Figure 6). This observation can be interpreted in terms of how the variances of the contributions of individual noise neurons are influenced by their respective firing rates and distances from the recording electrode. In order to simplify this interpretation, we assume that the noise contributing neurons are statistically independent and that the variance of the spike train from a given neuron is approximately linearly dependent on the neuron's firing rate. Then, at a given distance, a linear increase in firing rate will cause a linear increase in variance. Since spike amplitude decreases with distance as a power law, this linear increase in variance with an increase in firing rate will be larger as the distance becomes smaller.

Thus, if the variance of the spike train from the *n*-th neuron σ_n^2 relates to the neuron's firing rate f_n and the neuron's distance from the electrode r_n as a power law function of the distance, scaled with the firing rate, or

$$\sigma_n^2 \sim \frac{f_n}{r_n^m} \tag{16}$$

where m is the amplitude power law coefficient, the variance of the total recording (sum of all N spike train variances due to the statistical independence assumption) relates to the properties of the individual neurons as

$$\sigma_N^2 \sim \sum_{n=1}^{N} \frac{f_n}{r_n^m}. \tag{17}$$

Therefore, an overall increase in the firing rate of noise neurons makes the standard deviation of noise (the square root of the variance) more sensitive to an overall decrease in the distance to noise neurons.

Neuron	A_{min} (μV)	N_{pure}	N_{mixed}	I	(r_x, r_y, r_z) (μm)	(a_{far}, b_{far}) (μm^{-1}, unitless)
1	24	10	8	735	(53,58,104)	(6.8E-3,4.2)
2	18	16	8	753	(62,64,106)	(5.6E-3,4.3)
3	18	13	8	744	(65,78,142)	(7.4E-3,3.4)
4	22	24	6	397	(45,63,108)	(5.7E-3,4.1)

Table 1: A summary of derived model parameters. A_{min} is the spike amplitude threshold applied to determine the model ellipsoid volume. N_{pure} and N_{mixed} are the maximum orders of pure and mixed polynomial terms respectively and I is the resulting number of polynomial terms. (r_x, r_y, r_z) are the axial radii of the model ellipsoid and a_{far} and b_{far} are the coefficients of the amplitude decay power-law in the far field according to Equation 5.

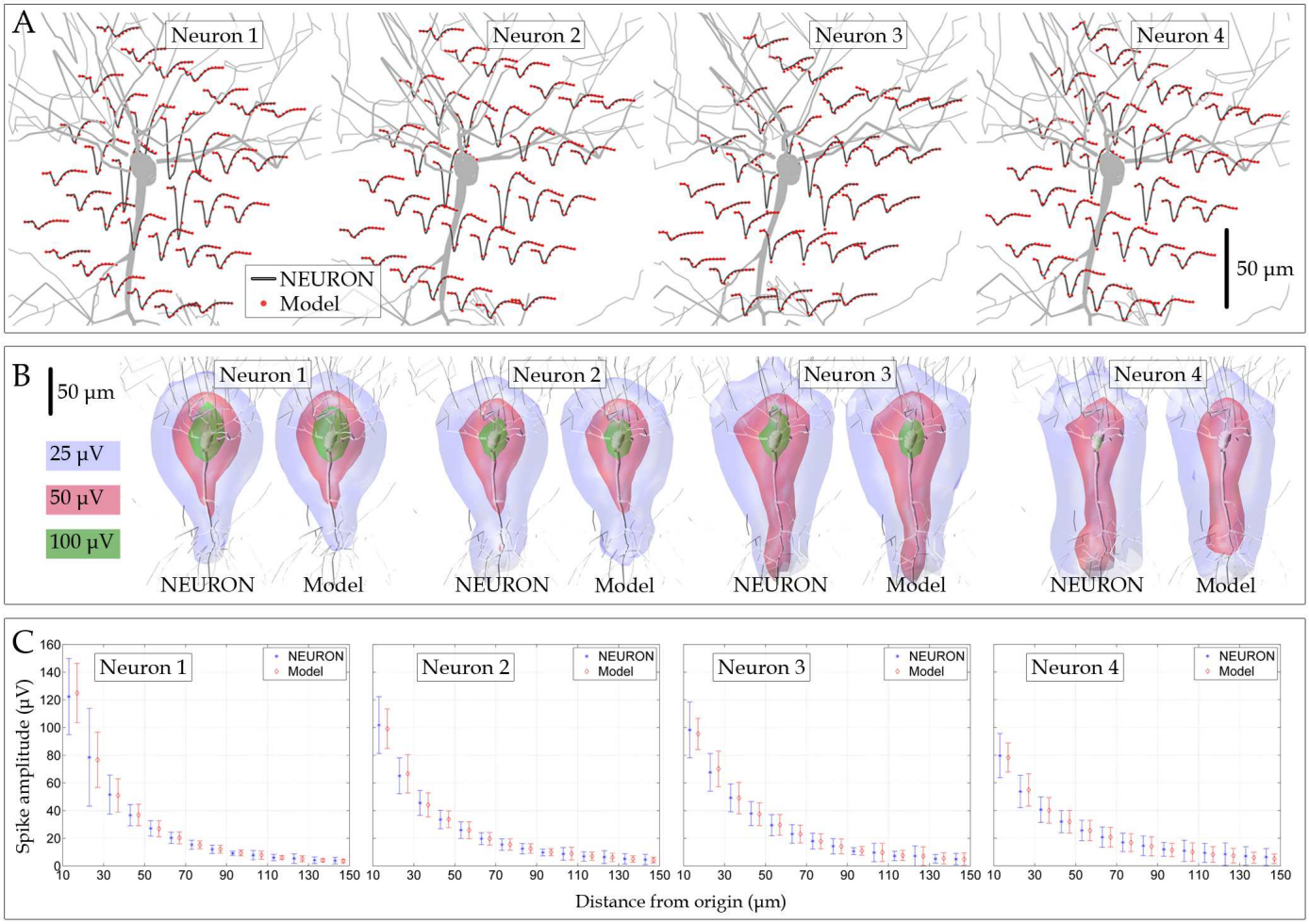

Figure 5: Validation of neuron models in terms of spike waveforms and spike amplitude. (A) Spike waveforms obtained with NEURON in an example set of measurement points (black) and spike waveforms calculated in those points by our models (red dots). (B) Spike amplitude fields displayed as spike amplitude isosurfaces at 25, 50 and 100 μV (blue, red and green respectively). (C) Spike amplitude (mean and standard deviation) as a function of distance from the origin (cell soma). The mean and standard deviation are taken across all spikes within 10 μm wide distance bins.

3.2.3. Application Example: Spike Sorting Performance

Figure 7 A shows the example recording scenario considered in our application example. The recorded signal at four example locations ($z = -20\mu m$, $z = 10\mu m$, $z = 30\mu m$ and $z = 50\mu m$) is shown in Figure 7 B along with extracted spike waveforms (mean waveforms ± standard deviation) for each of the four neurons at each of the four example locations. Figure 7 C shows the true and false positive classification rates (P_{TP} and P_{FP} for the individual neurons as well as the overall classification performance (P_{ID} and $1-P_{ID}$) as functions of the electrode position (z). Finally, Figure 7 D shows the PCA feature space development (first two PC weights) for the extracted spikes at ten example positions.

As expected, spike sorting performance varied significantly with the electrode position, both in terms of overall performance (P_{ID}) and for individual neurons (P_{TP} and P_{ID}). Overall performance (P_{ID}) was maximal at $z = 30\mu m$, which also appeared to generally provide the best performance with regard to individual neurons.

The example locations in Figure 7 A were selected to demon-

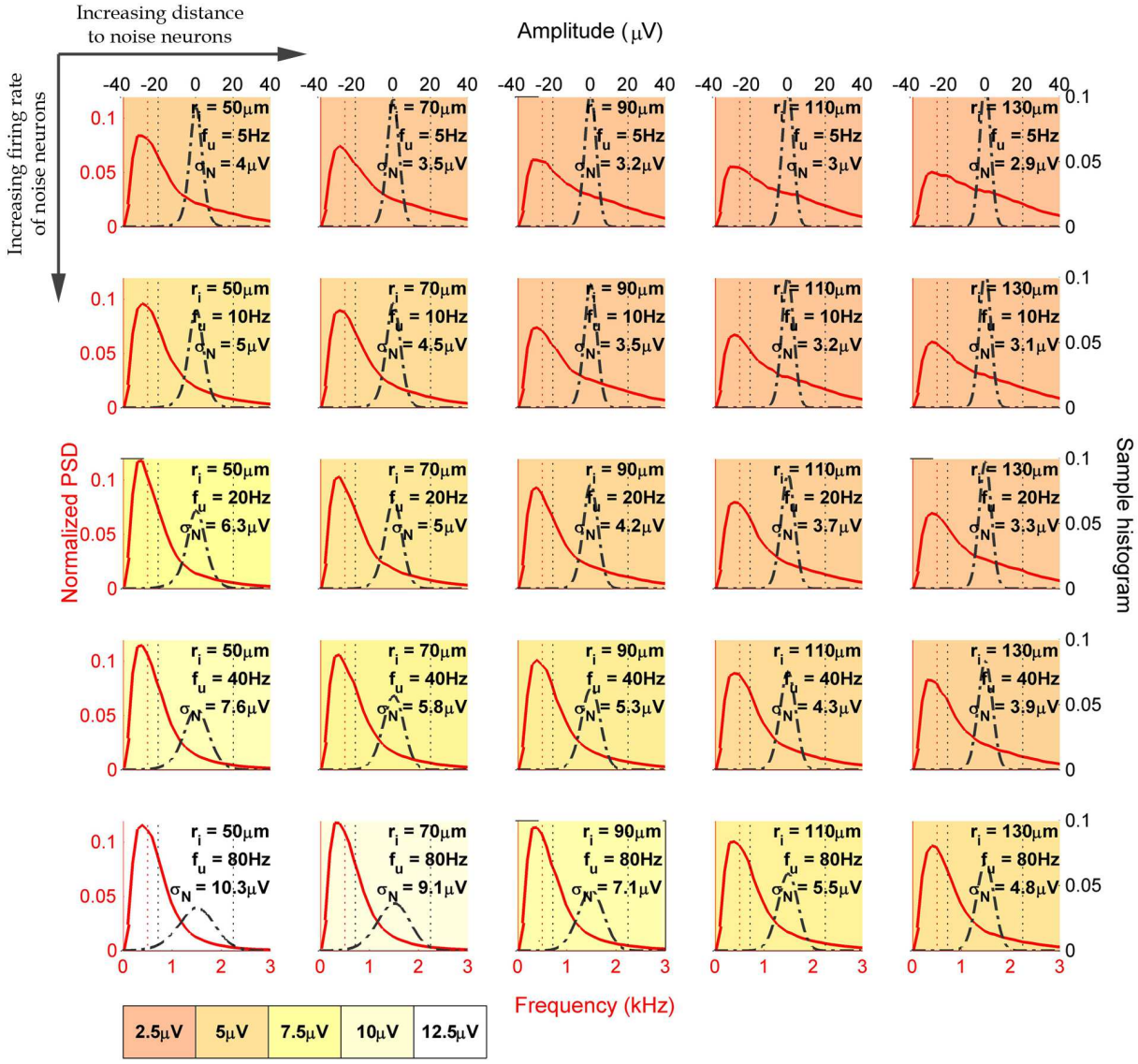

Figure 6: The recording noise properties as functions of the minimum distance of noise contributing neurons, r_i, and the upper limit of their firing rates, f_u. The individual firing rates of the neurons were selected from uniform distributions between 1 and f_u spikes/second. The red solid line show the normalized power spectral density (PSD) of the noise, the black broken line shows the sample histogram and the text inset shows the values of r_i and f_u for each case as well as the obtained standard deviation of the noise, σ_N for each case. The background color indicates the standard deviation of the noise.

strate the varying similarity between the spikes coming from different neurons, depending on the electrode position. At $z = -20\mu m$, the true positive classification rates (P_{TP}) were low for neurons 1 and 2 in comparison to neurons 3 and 4. At the same position, the false positive classification rates (P_{FP}) for neurons 1 and 2 were high. Also, the true and false positive classification rates for neuron 4 were almost maximal and minimal, respectively, and for neuron 3, essentially the same applied. At $z = 30\mu m$, all neurons had similar true and false positive classification rates, those being high and low respectively. At $z = 50\mu m$ however, the performance was low for neurons 1 and 3, but high for neurons 2 and 4.

This varying performance can be explained both in terms of the varying similarity between spike waveforms (Figure 7 B, right part) and how the PCA clusters develop as the electrode position is altered (Figure 7 D). At $z = -20\mu m$, the spike waveforms from neurons 1 and 2 were very similar and those from neuron 3 were somewhat similar to those from neurons 1 and 2. However, spikes from neuron 4 had a distinctive shape when compared to all other neurons. This is clearly seen in the PCA feature space where clusters 1 and 2 overlap heavily, cluster 3 is close to, but not overlapping clusters 1 and 2, and cluster 4 is well isolated from all other clusters.

At $z = 30\mu m$, all waveforms had distinctive characteristics, which was also reflected in the PCA feature space, where all clusters were well isolated. At $z > 30\mu m$, spikes from neurons 1 and 3 became more and more similar, which was seen in the PCA feature space as a gradually increased overlap between clusters 1 and 3.

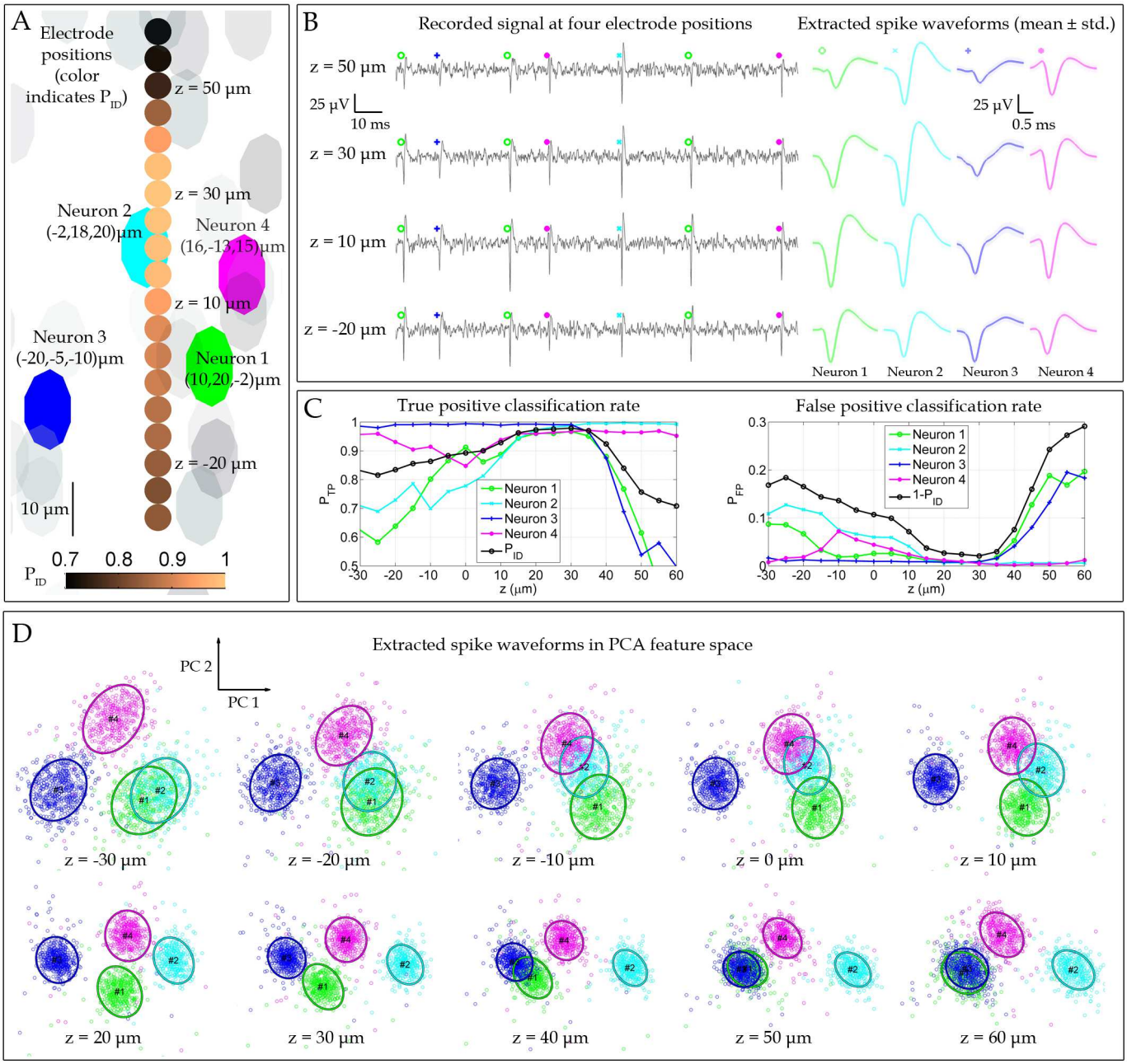

Figure 7: A demonstration of how our modeling and simulation can be used to evaluate spike sorting performance as a function of electrode position. (A) Nineteen electrodes (brown colored spheres along the center of the figure) were placed along the z axis ($x = y = 0$), each representing one electrode position to be evaluated. The electrodes were placed at $z = -30\mu m$ to $z = 60\mu m$ with a spacing of 5 μm. Four target neurons (neurons 1 to 4, green, light-blue, blue and purple ellipsoids) were placed close to the array of electrodes and noise neurons (gray ellipsoids) were placed far away. The size of the neurons corresponds approximately to the size of the cell soma in the NEURON model (see Figure 1). (B) Known spike times were used to extract spike waveforms from the recorded signals at each of the nineteen electrode locations and the extracted spike waveforms were sorted using principal component analysis (PCA) for feature extraction and K-means clustering for classification. (C) At each electrode location, true and false positive classification rates (P_{TP} and P_{FP}) were calculated for the individual neurons and the overall classification performance (P_{ID}) was estimated. (D) The first two dimensions of the PCA feature space development at every other electrode position, showing how the overlapping of the clusters varied with the electrode location. The varying overlapping of clusters in (D) and the varying similarities/dissimilarities between spike waveforms in (B) relate directly to the varying classification performance that is evident in (C).

4. Conclusions

In this paper we have described a novel approach for generating synthetic test signals to facilitate the development and testing of signal processing algorithms for neuronal signals. Our approach combines the powers of compartment models and template based signal models to provide a computationally and memory efficient way of simulating large scale recordings without discarding the spatial variability in spike waveforms. We have shown that we can use traditional compression tech-

niques to obtain a compact description of the spatial variability in measured spike waveforms predicted by compartment models and linear source approximations. The compressed models have been implemented into a simulation algorithm by which we generate synthetic spike trains as measured at an arbitrary number of electrode sites. The electrode sites can in turn be arbitrarily placed. The simulator has proved to be useful for providing synthetic multielectrode recordings in which the measured spike waveforms differ realistically between recording channels due to their different positions relative to the neurons. This property facilitates the development of algorithms for multichannel neuronal signal processing, the studying of the effects of electrode array geometry on the performance in information extraction and the studying of algorithms to handle moving electrodes.

We have performed the modeling for four different compartment models and our validation procedures have shown that despite the heavy compression, we can use the model to recreate the major features of the spatial variation in spike shape and amplitude. They also show that by adjusting the minimum distance and maximum firing rate of noise contributing neurons, we can control the amplitude and spectral properties of the physiological background noise.

We emphasize that the modeling procedure we have presented here is in not restricted to compartment models of pyramidal cells. Due to the generic character of our method, constructing a database of compressed models for various types of neurons would provide a way of efficiently simulating the measured neuronal activity in specific brain structures where multiple types of neurons might be present.

In the initial compartment model simulations we generated 42.875 spike waveforms (corresponding to the same number of measurement points), each being 100 samples of length. A file containing the spike waveforms in these discrete measurement points was thus roughly 31MB of size. With our compressed models we are able to obtain a file size of around 40kB, or 775 times smaller than the original data matrix. Besides being smaller in size, the model is not restricted to discrete coordinates and thus does not require any waveform interpolation for off-grid measurement points as would the initial spike waveforms from the compartment model.

To underline the computational efficiency of our simulation approach, we measured the time it took to generate recordings of various lengths with one and four simulated recording channels respectively. The measured simulation time was approximately 1.2 seconds/minute/channel and we tested recording lengths up to 16 minutes. In (Martinez et al., 2009) the authors reported that the simulation time was 270 seconds/minute for a single channel, or a factor 225 longer than what we observed with our simulator. With our previously reported simulator (Thorbergsson et al., 2009) we measured a simulation time of 16.5 seconds/minute for a single channel, or a factor of 13.75 times longer than the simulation time for the current simulator. Note that in contrast to the current simulation approach, the other simulators in this comparison neither capture the spatial variation in spike waveforms as a function of electrode position, nor do they facilitate the simulation of multiple electrode sites.

In comparison with other simulation approaches that have the ability to capture the spatial variation of spike waveforms, our simulator is significantly more efficient. An alternative approach would be to pre-calculate membrane currents for a given neuron model and use the LSA (Holt and Koch, 1999) to calculate spike waveforms in the given electrode locations, which corresponds to the first step in the modeling procedure presented in this paper. When initially calculating the LSA, we obtained simulation times of around 0.1 second/waveform. In the application example presented in Section 2.6, a total of 744 neurons were present (740 noise neurons and 4 target neurons) and 19 electrode sites – requiring the total number of $744 \times 19 = 14.136$ spike waveforms to be pre-calculated. Assuming direct scaling of calculation time with the number of waveforms, the direct LSA approach would require a total time of approximately 24 minutes to calculate all spike waveforms at all electrode sites. However, using our method, the entire set of 14.136 spike waveforms was calculated in approximately 2.4 seconds, or a factor of 600 times faster.

Another alternative approach would be to pre-calculate the LSA on a grid of measurement points and interpolate the waveforms for off-grid measurement points, as discussed in the Introduction (Franke et al., 2010b). However, interpolating such a high number of waveforms from a grid of 42.875 measurement points would be significantly more demanding than calculating the matrix multiplication of Equation 12.

Judging from our results, we conclude that our current simulator is both very computationally and memory efficient and offers increased realism in terms of spike waveform variability compared to current state-of-the-art simulators. Future work includes improving the user interface of the simulator and making it available to the research community as a tool for providing multi-channel test signals with realistic properties.

Acknowledgments

This work was supported by a Linnaeus Grant from the Swedish Research Council (no. 60012701), a grant from the Knut and Alice Wallenberg Foundation (no. 2004.0119) and the Medical and Engineering Faculties at Lund University.

References

Buzsáki G. Large-scale recording of neuronal ensembles. Nature Neuroscience 2004;7(5):446–51.

Duda R, Hart P, Stork D. Pattern classification. 2nd ed. Wiley, 2001.

Fee M, Mitra P, Kleinfeld D. Automatic sorting of multiple unit neuronal signals in the presence of anisotropic and non-gaussian variability. J Neurosci Methods 1996a;69(2):175–88.

Fee MS, Mitra PP, Kleinfeld D. Variability of extracellular spike waveforms of cortical neurons. J Neurophysiol 1996b;76(6):3823–33.

Franke F, Natora M, Boucsein C, Munk M, Obermayer K. An online spike detection and spike classification algorithm capable of instantaneous resolution of overlapping spikes. Journal of Computational Neuroscience 2010a;29:127–48.

Franke F, Natora M, Meier P, Hagen E, Pettersen K, Linden H, Einevoll G, Obermayer K. An automated online positioning system and simulation environment for multi-electrodes in extracellular recordings. In: Engineering

in Medicine and Biology Society (EMBC), 2010 Annual International Conference of the IEEE. IEEE; 2010b. p. 593–7.

Gold C, Henze D, Koch C. Using extracellular action potential recordings to constrain compartmental models. Journal of computational neuroscience 2007;23(1):39–58.

Gold C, Henze D, Koch C, Buzsáki G. On the origin of the extracellular action potential waveform: a modeling study. Journal of neurophysiology 2006;95(5):3113–28.

Harris KD, Henze DA, Csicsvari J, Hirase H, Buzsáki G. Accuracy of tetrode spike separation as determined by simultaneous intracellular and extracellular measurements. J Neurophysiol 2000;84(1):401–14.

Heeger D. Poisson model of spike generation. Technical Report; ; 2000.

Hines M, Carnevale N. The neuron simulation environment. Neural computation 1997;9(6):1179–209.

Holt G, Koch C. Electrical interactions via the extracellular potential near cell bodies. Journal of computational neuroscience 1999;6(2):169–84.

Lempka S, Johnson M, Moffitt M, Otto K, Kipke D, McIntyre C. Theoretical analysis of intracortical microelectrode recordings. Journal of Neural Engineering 2011;8. 045006.

Lewicki M. A review of methods for spike sorting: the detection and classification of neural action potentials. Network: Computation in Neural Systems 1998;9(4):R53–78.

Macke J, Berens P, Ecker A, Tolias A, Bethge M. Generating spike trains with specified correlation coefficients. Neural Computation 2009;21(2):397–423.

Martinez J, Pedreira C, Ison M, Quian Quiroga R. Realistic simulation of extracellular recordings. Journal of neuroscience methods 2009;184(2):285–93.

Obeid I, Wolf P. Evaluation of spike-detection algorithms for a brain-machine interface application. IEEE Transactions on Biomedical Engineering 2004;51(6):905–11.

Pettai R. Noise in receiving systems. Wiley-Interscience publication. Wiley, 1984.

Pettersen K, Einevoll G. Amplitude variability and extracellular low-pass filtering of neuronal spikes. Biophysical journal 2008;94(3):784–802.

Pouzat C, Mazor O, Laurent G. Using noise signature to optimize spike-sorting and to assess neuronal classification quality. Journal of neuroscience methods 2002;122(1):43–57.

Smith LS, Mtetwa N. A tool for synthesizing spike trains with realistic interference. Journal of Neuroscience Methods 2007;159(1):170–80.

The HDF Group . http://www.hdfgroup.org/. Webpage; 2012.

Thorbergsson P, Garwicz M, Schouenborg J, Johansson A. Statistical modelling of spike libraries for simulation of extracellular recordings in the cerebellum. In: Proc. 32nd Annual International Conference of the IEEE Engineering in Medicine and Biology Society EMBS 2010. IEEE; 2010. p. 4250–3.

Thorbergsson P, Jorntell H, Bengtsson F, Garwicz M, Schouenborg J, Johansson A. Spike library based simulator for extracellular single unit neuronal signals. In: Proc. 31st Annual International Conference of the IEEE Engineering in Medicine and Biology Society EMBS 2009. volume 1; 2009. p. 6998–7001.